

# A Deep Probabilistic Spatiotemporal Framework for Dynamic Graph Representation Learning with Application to Brain Disorder Identification

Junn Yong Loo<sup>1\*</sup> Sin-Yee Yap<sup>1\*</sup> Fuad Noman<sup>1</sup> Raphael CW Phan<sup>1</sup> Chee-Ming Ting<sup>1</sup>

## Abstract

Recent applications of pattern recognition techniques on brain connectome classification using functional connectivity (FC) neglect the non-Euclidean topology and causal dynamics of brain connectivity across time. In this paper, a deep probabilistic spatiotemporal framework developed based on variational Bayes (DSVB) is proposed to learn time-varying topological structures in dynamic brain FC networks for autism spectrum disorder (ASD) identification. The proposed framework incorporates a spatial-aware recurrent neural network to capture rich spatiotemporal patterns across dynamic FC networks, followed by a fully-connected neural network to exploit these learned patterns for subject-level classification. To overcome model overfitting on limited training datasets, an adversarial training strategy is introduced to learn graph embedding models that generalize well to unseen brain networks. Evaluation on the ABIDE resting-state functional magnetic resonance imaging dataset shows that our proposed framework significantly outperformed state-of-the-art methods in identifying ASD. Dynamic FC analyses with DSVB learned embeddings reveal apparent group difference between ASD and healthy controls in network profiles and switching dynamics of brain states.

brain regions, called the functional connectivity (FC). Alterations in resting-state FC networks have been associated with neuropsychiatric or neurodevelopmental disorders (Filippi et al., 2019), such as autism spectrum disorder (ASD) (Holiga et al., 2019; Valenti et al., 2020; Wang et al., 2021), schizophrenia (Nyatega et al., 2021; Liu et al., 2019), major depression (Zhu et al., 2020; Wang et al., 2020; Chen et al., 2021), and Alzheimer’s disease (Schumacher et al., 2019; Ahmadi et al., 2022).

Machine learning techniques have been applied to the identification and prediction of neuropsychiatric disorders in the past decade (Tanveer et al., 2020; Hyde et al., 2019). Traditional ML methods such as support vector machines (SVM), artificial neural networks, and deep learning methods are the most widely used ML techniques (Moridian et al., 2022). The notion of deep learning has especially gained popularity in the studies of neuroscience as it offers an opportunity to discover and understand the underlying differences in the pattern of brain connectivity between individuals with psychiatric disorders and healthy controls using deep neural networks (RaviPrakash et al., 2019; Khodatars et al., 2021; Zhang et al., 2020). For example, convolutional neural networks (CNN) (Kawahara et al., 2017a) are used to extract the high-level spatial dependencies present in the FC data; autoencoders (Cai et al., 2021; Yin et al., 2022) are utilized to learn the low-dimensional embeddings. However, these methods typically neglect the non-Euclidean (irregular and unordered topology) properties of the brain network.

Geometric Deep Learning (GDL) (Cao et al., 2020; Bronstein et al., 2017), a sub-branch of deep learning, has become popular in recent years to deal with more complex non-Euclidean data such as brain networks. The graph approach to GDL allows for great flexibility in modelling pairwise communications between brain regions at the subject level (Yan et al., 2019a), group-level relationships based on a population graph (Jiang et al., 2020a), or an ensemble of both (Li et al., 2022; Zhou & Zhang, 2021). However, these studies that use graph neural networks (GNNs) generally consider group-level network topology using phenotypic-based information, or use supervised subject-level embedding learning with pre-calculated population graphs for static brain network classification.

## 1. Introduction

The human brain is a complex system that consists of numerous interconnected neuronal regions. As revealed by functional magnetic resonance imaging (fMRI), spontaneous spatiotemporal fluctuations in brain activity exist even during a resting state (without any explicit task). Connectivity in brain networks is typically characterized via statistical dependence (such as correlations) between blood oxygen level dependent (BOLD) fMRI signals over spatially-distinct

<sup>\*</sup>Equal contribution <sup>1</sup>School of Information Technology, Monash University Malaysia. Correspondence to: Chee-Ming Ting <ting.cheeming@monash.edu>.

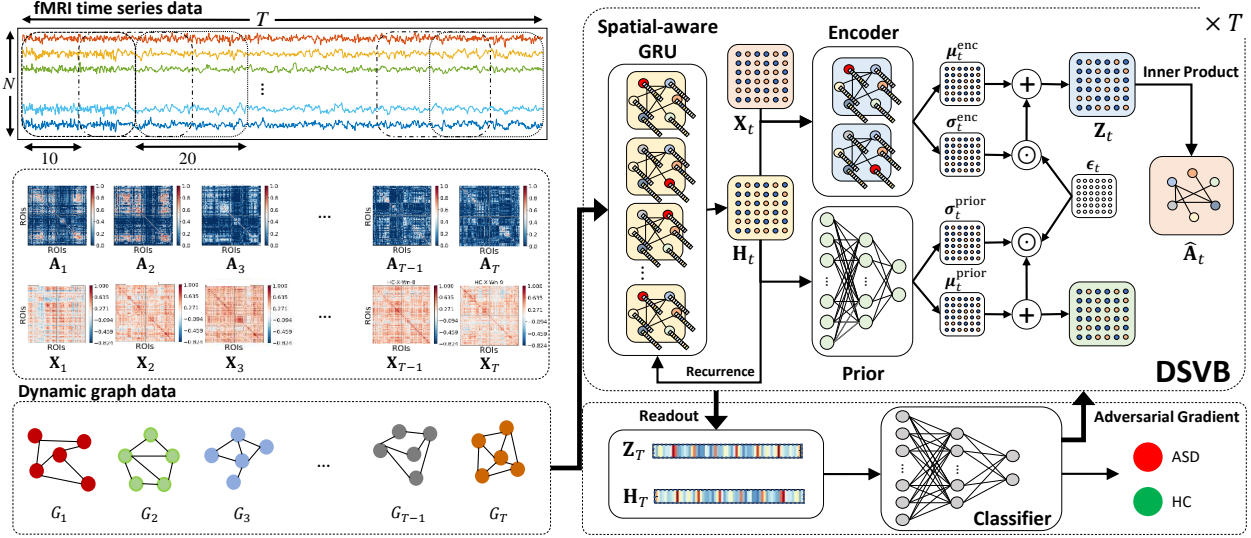


Figure 1. The architecture of the proposed DSVB framework for dynamic functional brain network classification.

Dynamicity of spatial patterns in resting-state brain functional networks across time has been reported in (Lee & Kim, 2019; Aedo-Jury et al., 2020). These studies show that it is important to consider not only the stationary topology of brain networks, but also the underlying dynamic temporal structure. Recent works (Noman et al., 2022; Liu et al., 2023) achieved this by incorporating graph convolutional network (GCN) to first learn spatial-aware graph embeddings of the dynamic FC, followed by a long short-term memory (LSTM) to leverage the temporal dependencies of these learned graph embeddings for subject-level network classification. Despite the promising results in revealing disrupted connectivity patterns, the segregated task-specific learning modules of these approaches inhibit their effectiveness in retaining the full spatiotemporal information of dynamic FC data throughout the spatial and temporal embedding layers. In addition, due to the deterministic nature of these existing models, they lack probabilistic interpretation and could fall short at modelling the stochastic variability of brain network data.

In this paper, a deep spatiotemporal variational Bayes (DSVB) framework is proposed to learn dynamic graph embeddings of dynamic FC networks, composed of sliding window segments of the resting-state fMRI time-series data. Fig. 1 shows an overview of the proposed DSVB framework for dynamic brain network classification. Derived from the general sequential variational Bayes (VB), our proposed framework intrinsically provides a stochastic representation modelling solution of the dynamic FC networks for neuropsychiatric disorder diagnosis. Unlike existing GNN-based approaches that learn independent and identically distributed (i.i.d.) graph embeddings, our proposed framework incorporates a spatial-aware recurrent neural network to accurately model both the complex topological structure and causal dependencies within a dynamic FC network se-

quence. Additionally, we introduce an adversarial training strategy to overcome the overfitting issue aggravated by limited training data.

To the best of our knowledge, this is the first work that investigates the feasibility of an end-to-end deep probabilistic spatiotemporal framework for dynamic graph representation learning and automated ASD identification. Our contributions are highlighted as follows:

1. An end-to-end probabilistic DSVB framework based on GNN is developed to learn a sequence stochastic graph embedding spaces in a purely unsupervised manner to accommodate a wide range of spatiotemporal variability across dynamic FC networks.
2. A spatial-aware Gated Recurrent Unit (GRU) is incorporated to generate hierarchical latent embeddings that extract underlying non-Euclidean topological structure and rich temporal patterns of a dynamic FC network sequence. The alterations in these latent embeddings are exploited for ASD identification via a fully-connected neural network (FCNN).
3. An adversarial model perturbation strategy is introduced to apply regularization on the GNN-based graph embedding models during training. This adversarial regularization facilitates learning of a smooth latent embedding space that extrapolates well to unseen dynamic FC networks beyond training dataset.
4. A nested-stratified 5-folds cross validation shows that our proposed framework outperforms state-of-the-art methods in ASD identification on a resting-state fMRI dataset of 144 subjects.

The rest of this paper is organised as follows. Section II introduces the formulation of the proposed DSVB framework.

Section III details the application of the DSVB framework to dynamic brain networks for ASD identification. Section IV presents and discusses the experimental results. Section V concludes the paper.

## 2. Methods

In this section, a probabilistic DSVB framework is developed to extract representative latent embeddings of the dynamic brain connectivity networks in a purely unsupervised manner. The extracted latent node embeddings are then used in a supervised downstream brain network classification task. An adversarial model perturbation strategy is finally introduced for the training of the proposed DSVB to prevent overfitting under limited training data.

### 2.1. Spatiotemporal Variational Bayes

In this subsection, we introduce a spatiotemporal variational Bayes objective that aims to maximize the variational evidence lower bound (ELBO) of log-likelihood  $\log p_\theta(\mathcal{A}|\mathcal{X})$  on a sequence of adjacency matrices  $\mathcal{A} = \{\mathbf{A}_t\}_{t=0}^T$  derived from dynamic brain networks, conditioned on the node features sequence  $\mathcal{X} = \{\mathbf{X}_t\}_{t=0}^T$  where  $T$  is the sequence length. By introducing a latent embeddings sequence  $\mathcal{Z} = \{\mathbf{Z}_t\}_{t=0}^T$ , the ELBO  $\mathcal{L}^{\text{ELBO}}(\theta, \vartheta)$  can be written via importance decomposition as

$$\mathcal{L}^{\text{ELBO}}(\theta, \vartheta) = \mathbb{E}_{q_\vartheta(\mathcal{Z}|\mathcal{X}, \mathcal{A})} \left[ \log \frac{p_\theta(\mathcal{A}, \mathcal{Z}|\mathcal{X})}{q_\vartheta(\mathcal{Z}|\mathcal{X}, \mathcal{A})} \right] \quad (1)$$

where the subscripts  $\theta$  and  $\vartheta$  denote GNN parameters that model the generative distribution  $p_\theta(\mathcal{A}, \mathcal{Z}|\mathcal{X})$  and the posterior distribution  $q_\vartheta(\mathcal{Z}|\mathcal{X}, \mathcal{A})$ , respectively.

Using the following general ancestral factorization:

$$\begin{aligned} p_\theta(\mathcal{A}, \mathcal{Z}|\mathcal{X}) &= \prod_{t=0}^T p_\theta(\mathbf{A}_t|\mathbf{Z}_{\leq t}, \mathbf{X}_{< t}, \mathbf{A}_{< t}) \times \\ &\quad p_\theta(\mathbf{Z}_t|\mathbf{X}_{< t}, \mathbf{A}_{< t}, \mathbf{Z}_{< t}) \\ q_\vartheta(\mathcal{Z}|\mathcal{X}, \mathcal{A}) &= \prod_{t=0}^T q_\vartheta(\mathbf{Z}_t|\mathbf{X}_{\leq t}, \mathbf{A}_{\leq t}, \mathbf{Z}_{< t}) \end{aligned} \quad (2)$$

we can expand (1) to obtain the sequential ELBO (sELBO) as follows:

$$\begin{aligned} \mathcal{L}^{\text{sELBO}}(\theta, \vartheta) &= \\ &\sum_{t=0}^T \left[ \mathbb{E}_{q_\vartheta(z_{\leq t}|\mathbf{x}_{\leq t})} \left[ \log p_\theta(\mathbf{A}_t|\mathbf{Z}_{\leq t}, \mathbf{X}_{< t}, \mathbf{A}_{< t}) \right] \right. \\ &\quad \left. - \mathcal{D}^{\text{KL}}[q_\vartheta(\mathbf{Z}_t|\mathbf{X}_{\leq t}, \mathbf{A}_{\leq t}, \mathbf{Z}_{< t}) \| p_\theta(\mathbf{Z}_t|\mathbf{X}_{< t}, \mathbf{A}_{< t}, \mathbf{Z}_{< t})] \right] \end{aligned} \quad (3)$$

where  $\mathbf{X}_{\leq t}$  and  $\mathbf{X}_{< t}$  denote the partial sequences up to the  $t^{\text{th}}$  and  $(t-1)^{\text{th}}$  time samples, respectively.  $\mathcal{D}^{\text{KL}}$  denotes

the (positive-valued) Kullback–Leibler divergence (KLD). The conditional probabilities of (3) encapsulate the underlying causal structure and temporal coherence of the dynamic brain networks. This sELBO forms the basis of our proposed DSVB framework.

### 2.2. Recurrent Graph Neural Network

In this subsection, we introduce a model parameterization based on graph recurrent neural network for the sELBO (3). The conditional latent prior and approximate posterior in (2) are first assumed to be Gaussian distributions:

$$p_\theta(\mathbf{Z}_t|\mathbf{X}_{< t}, \mathbf{A}_{< t}, \mathbf{Z}_{< t}) = \mathcal{N}(\boldsymbol{\mu}_t^{\text{prior}}, \boldsymbol{\Sigma}_t^{\text{prior}}) \quad (4a)$$

$$q_\vartheta(\mathbf{Z}_t|\mathbf{X}_{\leq t}, \mathbf{A}_{\leq t}, \mathbf{Z}_{< t}) = \mathcal{N}(\boldsymbol{\mu}_t^{\text{enc}}, \boldsymbol{\Sigma}_t^{\text{enc}}) \quad (4b)$$

with isotropic covariances  $\boldsymbol{\Sigma}_t^{\text{prior}} = \text{Diag}(\sigma_t^{\text{prior}^2})$ ,  $\boldsymbol{\Sigma}_t^{\text{enc}} = \text{Diag}(\sigma_t^{\text{enc}^2})$ , and  $\text{Diag}(\cdot)$  denotes the diagonal function.

To allow gradient descent optimization of sELBO (3), the mean and standard deviation pairs in (4) are modelled as

$$(\boldsymbol{\mu}_t^{\text{prior}}, \boldsymbol{\Sigma}_t^{\text{prior}}) = \varphi_\theta^{\text{prior}}(\mathbf{H}_t) \quad (5a)$$

$$(\boldsymbol{\mu}_t^{\text{enc}}, \boldsymbol{\Sigma}_t^{\text{enc}}) = \Phi_\vartheta^{\text{enc}}(\varphi_\theta^x(\mathbf{X}_t), \mathbf{H}_t, \mathbf{A}_t) \quad (5b)$$

where the prior model  $\varphi_\theta^{\text{prior}}$ , the measurement feature model  $\varphi_\theta^x$ , and the state feature model  $\varphi_\theta^z$  are modelled as FCNNs; the encoder model  $\Phi_\vartheta^{\text{enc}}$  is modelled as GNN. The memory-embedding recurrent states  $\mathbf{H}_t$  in (5) are obtained via

$$\mathbf{H}_t = \Phi_\theta^{\text{mn}}(\varphi_\theta^x(\mathbf{X}_{t-1}), \varphi_\theta^z(\mathbf{Z}_{t-1}), \mathbf{H}_{t-1}, \mathbf{A}_{t-1}) \quad (6)$$

where the recurrent model  $\Phi_\theta^{\text{mn}}$  is modelled as a spatial-aware Gated Recurrent Unit (GRU). By virtue of (6),  $\mathbf{H}_t$  thus serve as the memory embeddings for history path  $\{\mathbf{Z}_{\leq t}, \mathbf{X}_{< t}, \mathbf{A}_{< t}\}$ .

Subsequently, we let the adjacency matrix likelihood in (2) be a Bernoulli distribution:

$$p_\theta(\mathbf{A}_t|\mathbf{Z}_{\leq t}, \mathbf{X}_{< t}, \mathbf{A}_{< t}) = \text{Bernoulli}(\hat{\mathbf{A}}_t) \quad (7)$$

where  $\hat{\mathbf{A}}_t$  is the adjacency matrix reconstruction obtained via the following inner product with sigmoid activation:

$$\hat{\mathbf{A}}_t = \sigma([\mathbf{Z}_t, \mathbf{H}_t] [\mathbf{Z}_t, \mathbf{H}_t]^\top) \quad (8)$$

In particular, we allow the adjacency matrix likelihood to be conditioned on the entire history path, which suggested the incorporation of memory-embedding  $\mathbf{H}_t$  in the inner-product decoder (8), as opposed to the variational graph recurrent neural network (Hajiramezanali et al., 2019) which only considered  $\mathbf{Z}_t$ .

Substituting (8) into (7), the adjacency matrix log-likelihood  $\log p_\theta(\mathbf{A}_t|\mathbf{Z}_{\leq t}, \mathbf{X}_{< t}, \mathbf{A}_{< t})$  can be written in the form of

negative binary cross entropy (BCE):

$$\begin{aligned} \mathcal{L}^{\text{BCE}}(\theta, \vartheta) = & \sum_{i,j=1}^{N,D} \left[ a_{t,ij} \log \sigma([\mathbf{Z}_{t,i}, \mathbf{H}_{t,i}] [\mathbf{Z}_{t,j}, \mathbf{H}_{t,j}]^\top) \right. \\ & \left. + (1 - a_{t,ij}) \log (1 - \sigma([\mathbf{Z}_{t,i}, \mathbf{H}_{t,i}] [\mathbf{Z}_{t,j}, \mathbf{H}_{t,j}]^\top)) \right] \end{aligned} \quad (9)$$

where  $x_{t,ij}$  denotes the  $(i, j)^{\text{th}}$  element of matrix  $\mathbf{X}_t$ , and  $\mathbf{X}_{t,i}$  denotes the  $i^{\text{th}}$  row of matrix  $\mathbf{X}_t$ . Given that the ground-truth adjacency matrices  $\{\mathbf{A}_t\}_{t=0}^T$  are sparse, we consider only their non-zero elements (i.e.,  $a_{t,ij} > 0$ ) in (9). This BCE thus acts as the reconstruction loss between non-zero elements of the estimated  $\hat{\mathbf{A}}_t$  and the ground-truth  $\mathbf{A}_t$ . Subsequently, we approximate the first expectation term in (3) via Monte Carlo integration as follows:

$$\begin{aligned} \mathbb{E}_{q_\vartheta(z_{\leq t} | x_{\leq t})} [\log p_\theta(\mathbf{A}_t | \mathbf{Z}_{\leq t}, \mathbf{X}_{\leq t}, \mathbf{A}_{< t})] \\ = \frac{1}{M} \sum_{k=1}^M \mathcal{L}^{\text{BCE}}(\mathbf{Z}_t^k, \mathbf{H}_t^k) \end{aligned} \quad (10)$$

where  $k$  denotes the particle index, and  $M$  is the number of particles which can be set to 1 when mini-batch size is sufficiently large (Kingma & Welling, 2014).

The latent particles  $\mathbf{Z}_t^k \sim q_\vartheta(\mathbf{Z}_t | \mathbf{X}_{\leq t}, \mathbf{A}_{\leq t}, \mathbf{Z}_{< t})$  are obtained via (5b) using the reparameterization trick  $\mathbf{Z}_t^k = \boldsymbol{\mu}_t^{\text{enc},k} + \mathbf{s}_t^{\text{enc},k} \odot \boldsymbol{\epsilon}_t^k$ , where  $\boldsymbol{\epsilon}_t^k \sim \mathcal{N}(\mathbf{0}, \mathbf{I})$  and  $\odot$  denotes the Hadamard (element-wise) product. The recurrent state particles  $\mathbf{H}_t^k$  are obtained via (6) given the previous time-step  $\mathbf{Z}_{t-1}^k$  and  $\mathbf{H}_{t-1}^k$ .

Besides, a closed-form solution of the KLD  $\mathcal{D}^{\text{KL}}$  in sELBO (3) can be analytically obtained as

$$\begin{aligned} \mathcal{D}^{\text{KL}}(\theta, \vartheta) = & \mathbb{E}_{q_\vartheta(\mathbf{Z}_t | \mathbf{X}_{\leq t}, \mathbf{A}_{\leq t}, \mathbf{Z}_{< t})} \left[ \log \frac{\mathcal{N}(\boldsymbol{\mu}_t^{\text{enc}}, \boldsymbol{\Sigma}_t^{\text{enc}})}{\mathcal{N}(\boldsymbol{\mu}_t^{\text{prior}}, \boldsymbol{\Sigma}_t^{\text{prior}})} \right] \\ = & \frac{1}{2} \sum_{i,j=1}^{N,D} \left[ \frac{s_{t,ij}^{\text{enc}^2}}{s_{t,ij}^{\text{prior}^2}} - \log \frac{s_{t,ij}^{\text{enc}^2}}{s_{t,ij}^{\text{prior}^2}} + \frac{(\mu_{t,ij}^{\text{enc}} - \mu_{t,ij}^{\text{prior}})^2}{s_{t,ij}^{\text{prior}^2}} - 1 \right] \end{aligned} \quad (11)$$

which is deterministic and thus circumvents MC approximation. This KLD loss thus measures the statistical distance between the conditional prior (4a) and approximate posterior (4b). Its optimization enforces latent space that exhibits strong causality due to the emphasis of the prior (5a) on the preceding graphs and embeddings  $\{\mathbf{X}_{< t}, \mathbf{A}_{< t}, \mathbf{Z}_{< t}\}$ .

By substituting (9) and (11) into (3), we establish an unsupervised sELBO loss that underpins the proposed DSVB framework. To sum up, the end-to-end prior (5a), encoder (5b), recurrent (6) and inner-product decoder (8) constitute a probabilistic recurrent graph autoencoder (GAE) that first

constructs sequential stochastic hierarchical latent embedding spaces on  $\{\mathbf{Z}_t, \mathbf{H}_t\}_{t=0}^T$ , and then uses the sampled embeddings  $\{\mathbf{Z}_t^k, \mathbf{H}_t^k\}_{k=0}^M$  to obtain stochastic estimation  $\{\hat{\mathbf{A}}_t\}_{t=0}^T$  of the adjacency matrices. By optimizing sELBO (3) with respect to the model parameters  $\{\theta, \vartheta\}$ , these embedding spaces learn to accommodate an extensive range of stochastic spatiotemporal variability across dynamic brain networks in a purely unsupervised manner.

### 2.3. Attention-based Message Passing and Spatial-aware Gated Recurrent Unit

GNN is a class of message passing neural networks that uses aggregated topological information to construct and update node-level graph embeddings. In our proposed DSVB, we consider a GNN with message passing scheme inspired by the multi-head attention mechanism in the Transformer (Vaswani et al., 2017), of which the node embeddings are updated across layers as follows:

$$\mathbf{h}_i^{(l+1)} = \mathbf{W}_1 \mathbf{h}_i^{(l)} + \sum_{j \in \mathcal{N}(i)} \alpha_{ij} (\mathbf{W}_2 \mathbf{h}_j^{(l)} + \mathbf{W}_5 \mathbf{h}_{ij}) \quad (12)$$

and  $\alpha_{ij}$  are the attention coefficients computed as

$$\alpha_{ij} = \text{softmax} \left( \frac{(\mathbf{W}_3 \mathbf{h}_i^{(l)})^\top (\mathbf{W}_4 \mathbf{h}_j^{(l)} + \mathbf{W}_5 \mathbf{h}_{ij})}{\sqrt{D_{l+1}}} \right) \quad (13)$$

with learnable weights  $\{\mathbf{W}_1, \mathbf{W}_2, \dots, \mathbf{W}_5\}$  that project the embeddings from  $\mathbb{R}^{D_l}$  to  $\mathbb{R}^{D_{l+1}}$ , and  $\mathbf{h}_i^{(l)}$  denotes the node embeddings at the  $l^{\text{th}}$  GNN layer.

It follows from the scaled dot product (13) that the node embeddings  $\mathbf{h}_i$  and its neighbors  $\mathbf{h}_j$  can be interpreted as the ‘query’ and ‘key’ of a self-attention mechanism. The edge features are added to the key vectors in order to provide an additional source of information for the node. After that, a similarity measure between the query and keys is calculated via dot product to obtain the coefficients  $\alpha_{ij}$ , which act as attention scores in the feature aggregation step of (12). The encoder model (5b) of our proposed DSVB is thus modelled as by a two-layered GNN with this message passing scheme, and we let  $\mathbf{h}^{(0)} = [\varphi_\theta^x(\mathbf{X}_t), \mathbf{H}_t, \mathbf{A}_t]^\top$  and  $\mathbf{h}^{(2)} = [\boldsymbol{\mu}_t^{\text{enc}}, \boldsymbol{\Sigma}_t^{\text{enc}}]^\top$  in (12).

To accurately model spatiotemporal dependencies, we parameterize the recurrent model (6) using a spatial-aware GRU, for which the recurrent states are updated across time-steps as follows:

$$\begin{aligned} \mathbf{S}_t &= \sigma(\Phi_{xz}(\mathbf{X}, \mathbf{A}) + \Phi_{hz}(\mathbf{H}_{t-1}, \mathbf{A})) \\ \mathbf{R}_t &= \sigma(\Phi_{xr}(\mathbf{X}, \mathbf{A}) + \Phi_{hr}(\mathbf{H}_{t-1}, \mathbf{A})) \\ \tilde{\mathbf{H}}_t &= \tanh(\Phi_{xh}(\mathbf{X}, \mathbf{A}) + \Phi_{hh}(\mathbf{R}_t \odot \mathbf{H}_{t-1}, \mathbf{A})) \\ \mathbf{H}_t &= \mathbf{S}_t \odot \mathbf{H}_{t-1} + (1 - \mathbf{S}_t) \odot \tilde{\mathbf{H}}_t \end{aligned} \quad (15)$$



$$\begin{aligned}
 \mathcal{L}^{\text{DSVB-FCNN}}(\theta, \vartheta, \tau) &= \mathcal{L}^{\text{BCE}}(\theta, \vartheta) + \mathcal{D}^{\text{KL}}(\theta, \vartheta) + \mathcal{L}^{\text{CE}}(\tau) \\
 &= \frac{1}{M} \sum_{t=0}^T \sum_{k=1}^M \sum_{i,j=1}^{N,D} \left[ a_{t,ij} \log \sigma([\mathbf{Z}_{t,i}^k, \mathbf{H}_{t,i}^k][\mathbf{Z}_{t,j}^k, \mathbf{H}_{t,j}^k]^\top) - (1 - a_{t,ij}) \log (1 - \sigma([\mathbf{Z}_{t,i}^k, \mathbf{H}_{t,i}^k][\mathbf{Z}_{t,j}^k, \mathbf{H}_{t,j}^k]^\top)) \right] \\
 &\quad \underbrace{\hspace{10em}}_{\mathcal{L}^{\text{BCE}}(\theta, \vartheta)} \\
 &\quad + \frac{1}{2} \sum_{t=0}^T \sum_{i,j=1}^{N,D} \left[ \frac{s_{t,ij}^{\text{enc}^2}}{s_{t,ij}^{\text{prior}^2}} - \log \frac{s_{t,ij}^{\text{enc}^2}}{s_{t,ij}^{\text{prior}^2}} + \frac{(\mu_{t,ij}^{\text{enc}} - \mu_{t,ij}^{\text{prior}})^2}{s_{t,ij}^{\text{prior}^2}} - 1 \right] + \sum_{i=1}^C c_i \log \frac{\exp(\hat{y}_i)}{\sum_{j=1}^C \exp(\hat{y}_j)} \\
 &\quad \underbrace{\hspace{10em}}_{\mathcal{D}^{\text{KL}}(\theta, \vartheta)} \quad \underbrace{\hspace{10em}}_{\mathcal{L}^{\text{CE}}(\tau)}
 \end{aligned} \tag{14}$$

where we let  $\mathbf{X} = [\varphi_\theta^x(\mathbf{X}_{t-1}), \varphi_\theta^z(\mathbf{Z}_{t-1})]^\top$  and  $\mathbf{A} = \mathbf{A}_{t-1}$ . By virtue of (15),  $\mathbf{H}_t$  thus serve as memory embeddings that retain graph-structured temporal information of the preceding latent state sequence  $\mathbf{Z}_{<t}$ . In comparison to conventional GRU, the FCNN therein is replaced by the set of GNNs  $\{\Phi_{xz}, \Phi_{hz}, \Phi_{xr}, \Phi_{hr}, \Phi_{xh}, \Phi_{hh}\}$ . Similarly, these single-layered GNNs adopt the message passing scheme in (12) which allows the modified GRU to simultaneously exploit meaningful spatial structures and temporal dependencies of the dynamic graph-structured data.

#### 2.4. Latent Embeddings for Graph Classification

Due to the recurrent nature of our proposed DSVB, the generated latent embeddings preserve non-Euclidean topological structure and rich temporal patterns which can be further exploited for dynamic graph classification. In combination, these node embeddings entail crucial spatiotemporal information of the entire dynamic graph sequence. To summarize the subject-level dynamic graphs, we apply a flattening operation on the mean of hierarchical embeddings  $\mathbf{Z}_T, \mathbf{H}_T$  of the final time-step  $T$  to obtain the vectorized readout  $\text{vec}([\mu_T^{\text{enc}}, \mu_T^{\text{H}}]^\top)$  with  $\mu_T^{\text{H}} = \frac{1}{M} \sum_{k=1}^M \mathbf{H}_T^k$ .

Subsequently, the flattened readout is fed into the following classification model:

$$\hat{\mathbf{y}} = \varphi_\tau^{\text{classifier}}(\text{vec}[\mu_T^{\text{enc}}, \mu_T^{\text{H}}]^\top) \tag{16}$$

modelled by multilayer FCNN. A softmax activation is then applied on the obtained logits  $\hat{\mathbf{y}} \in \mathbb{R}^2$  to obtain the predictive probability scores for the final subject-level brain network classification. The predicted class label is thus the one with highest predictive score. The classification loss is taken to be the following multi-class cross entropy:

$$\mathcal{L}^{\text{CE}}(\tau) = \sum_{i=1}^C c_i \log \frac{\exp(\hat{y}_i)}{\sum_{j=1}^C \exp(\hat{y}_j)} \tag{17}$$

where  $\mathbf{c} \in \{0, 1\}^C$  is the class label and  $C$  is the number of classes. Incorporating (17) to the sELBO (3), we obtain the final DSVB-FCNN loss  $\mathcal{L}^{\text{DSVB}}$  in (14).

Unlike previous methods, the FCNN classifier (16) is trained jointly with the variational recurrent graph autoencoder (5)-(6) in an end-to-end fashion. Gradients of the classifier are allowed to back-propagate through time and update parameters  $\{\theta, \vartheta\}$  of the DSVB models.

#### 2.5. Adversarial Model Regularization

Under a limited amount of training data, deep graph representation learning models are prone to generating node embeddings that aggravate overfitting. These models construct a latent embedding space that is exceedingly conformed to the limited dataset. Consequently, downstream task-specific (e.g. graph classification) models that are adapted to this data-specific latent space perform poorly on unseen latent embeddings of general graphs.

Taking this into consideration, a probabilistic adversarial training strategy is introduced to regularize the latent embedding space constructed by the DSVB models. With the adversarial regularization, the DSVB models are expected to overcome the data overfitting issue by realizing a more inclusive latent embedding space that can be readily extrapolated to unseen data beyond the limited training dataset.

Inspired by the model perturbation strategy in domain adversarial training (Ganin et al., 2016), we train the parameters  $\{\theta, \vartheta, \tau\}$  of DSVB-FCNN loss (14) in an adversarial fashion as follows:

$$\begin{aligned}
 (\theta, \vartheta) &= \arg \max_{\theta, \vartheta} \mathcal{L}^{\text{DSVB-FCNN}}(\theta, \vartheta, \tau) \\
 \tau &= \arg \min_{\tau} \mathcal{L}^{\text{DSVB-FCNN}}(\theta, \vartheta, \tau)
 \end{aligned} \tag{18}$$

On one hand, the DSVB parameters  $(\theta, \vartheta)$  are optimized to generate hierarchical embeddings  $\mathbf{Z}_T, \mathbf{H}_T$  that fool the classifier  $\varphi_\tau^{\text{classifier}}$ . On the other hand, the FCNN classification model parameters  $\tau$  are optimized to accurately distinguish the class label of the generated latent embeddings. Such an adversarial competition is expected to achieve the Nash equilibrium that generalizes the latent embedding space and prevents model overfitting.

Table 1. Performance comparison of the proposed DSVB-FCNN with different static and dynamic baseline classifiers based on a nested-stratified 5-folds cross validation.

Type of FC	Classifier	Accuracy (%)	Recall (%)	Precision (%)	F1-Score (%)	AUC (%)
Static	SVM	56.26 ± 4.51	55.71 ± 3.19	55.05 ± 4.69	55.37 ± 3.97	56.24 ± 3.99
	BrainNetCNN (Kawahara et al., 2017b)	57.04 ± 10.99	44.29 ± 15.29	61.52 ± 15.24	49.03 ± 13.10	56.62 ± 10.86
	ASD-DiagNet (Eslami et al., 2019)	68.03 ± 2.87	58.57 ± 12.29	74.04 ± 10.60	63.55 ± 4.05	67.62 ± 2.64
	GroupINN (Yan et al., 2019b)	64.53 ± 9.06	34.29 ± 24.49	67.88 ± 35.09	43.10 ± 25.83	63.76 ± 9.37
	Hi-GCN (Jiang et al., 2020b)	66.60 ± 6.05	60.00 ± 10.69	68.51 ± 7.19	63.30 ± 6.74	66.38 ± 6.06
	E-Hi-GCN (Li et al., 2021)	66.60 ± 8.64	54.29 ± 21.48	75.42 ± 14.71	58.31 ± 18.40	58.00 ± 6.38
Dynamic	SVM	63.82 ± 9.41	55.43 ± 7.23	56.66 ± 3.34	55.52 ± 3.61	63.52 ± 8.20
	BrainNetCNN (Kawahara et al., 2017b)	54.49 ± 8.15	57.14 ± 8.34	50.00 ± 14.00	53.33 ± 10.15	54.58 ± 7.03
	GAE-FCNN (Noman et al., 2022)	66.03 ± 7.14	65.71 ± 14.57	68.92 ± 16.26	64.96 ± 6.37	66.19 ± 7.17
	GAE-LSTM (Noman et al., 2022)	54.78 ± 6.05	47.14 ± 19.48	71.00 ± 25.12	54.92 ± 17.09	54.53 ± 6.13
	<b>DSVB-FCNN</b>	<b>78.44 ± 2.77</b>	<b>66.67 ± 7.45</b>	<b>89.64 ± 5.90</b>	<b>75.99 ± 4.01</b>	<b>78.94 ± 2.64</b>

Table 2. Ablation study of the proposed DSVB framework based on a nested-stratified 5-folds cross validation.

Model	Specification	Accuracy (%)	Recall (%)	Precision (%)	F1-Score (%)	AUC (%)
I	Graph Autoencoder + Conventional GRU	72.39 ± 9.01	65.00 ± 8.16	78.91 ± 13.04	71.02 ± 9.05	72.65 ± 9.08
II	Graph Autoencoder + Spatial-aware GRU	76.63 ± 9.08	73.33 ± 8.16	82.05 ± 11.47	76.74 ± 7.47	76.74 ± 9.32
III	Variational Graph Autoencoder + Spatial-aware GRU	75.00 ± 10.06	63.33 ± 6.67	86.94 ± 15.26	72.78 ± 8.90	75.38 ± 10.31
IV	Graph Autoencoder + Spatial-aware GRU + Adversarial Training	77.61 ± 5.65	<b>76.67 ± 6.24</b>	79.48 ± 6.45	<b>77.96 ± 5.73</b>	77.65 ± 5.67
V	Variational Graph Autoencoder + Spatial-aware GRU + Adversarial Training	<b>78.44 ± 2.77</b>	66.67 ± 7.45	<b>89.64 ± 5.90</b>	75.99 ± 4.01	<b>78.94 ± 2.64</b>

### 3. Application to Dynamic Brain Networks

#### 3.1. fMRI Dataset & Preprocessing

We used a subset of C-PAC pipeline (Cameron et al., 2013) preprocessed fMRI dataset from the Autism Brain Imaging Data Exchange (ABIDE I) open source database (Di Martino et al., 2009), with a total of 144 (70 ASD and 74 healthy controls (HC)) resting-state fMRI time-series included in this case study. The inclusion criteria are: males with a full-scale IQ > 80; ages between 11 and 23; and fMRI acquisition sites are New York University, University of California Los Angeles 1, and University of Utah, School of Medicine. We performed parcellation using Power et al.’s brain atlas (Power et al., 2011) to extract the mean time series for a total of  $N = 264$  regions of interest (ROIs).

#### 3.2. Dynamic Brain Network Construction

Dynamic brain graphs were constructed from fMRI data using the sliding-window technique. The fMRI ROI time series was segmented into multiple overlapping blocks using sliding windows of size  $L = 20$  with shift of 10 time-steps. To represent the dynamic FC networks, we computed correlation matrix between ROI time series for each time window. Ledoit-Wolf (LDW) regularized shrinkage covariance estimator is used to ensure well-conditioned FC estimates.

The dynamic brain network at each time-step  $t$  is denoted as  $G_t \equiv (V, E)$  where  $v_i \in V$  represents a particular brain ROI and  $e_{ij} \in E$  is the connectivity edge between a pair of nodes  $v_i$  and  $v_j$ . The topological structure of dynamic brain networks  $G_t$  can be represented by a sequence of time-resolved adjacency matrices  $\mathbf{A}_t = [a_{t,ij}] \in \{0, 1\}^{N \times N}$ , which were constructed by proportional thresholding of the sliding-windowed correlation-based FC matrices to

keep the strongest 40% connections based on absolute correlation value, and setting other connections to zeros. Each dynamic graph  $G_t$  has an associated node features  $\mathbf{X}_t = [\mathbf{x}_{t,1}, \dots, \mathbf{x}_{t,N}]^T \in \mathbb{R}^{N \times D}$  where  $\mathbf{x}_{t,i}$  is the feature vector for node  $v_i$ . We used the connection weights of each node for  $\mathbf{x}_{t,i}$ .

#### 3.3. Graph Neural Network Model Training

The proposed DSVB framework is used to generate the dynamic node embeddings that correspond to the node feature and adjacency matrix sequences. The FCNN classifier is then used to discriminate between the ASD and HC subjects. We train the end-to-end DSVB-FCNN via an Adam optimizer using a learning rate of 0.00001 with annealing and a l2 regularization of 0.01 for 400 epochs. The output dimension of the graph-structure GRU is chosen to be 16. The output dimensions of each layer of the GNN encoder are chosen to be 32 and 16, respectively. The output dimensions of the single-layered FCNN measurement and state feature models are chosen to be 64 and 8, respectively. The output dimensions of each layer of the FCNN classifier is chosen to be 32 and 2, respectively. These model hyperparameters are selected based on a 5-folds cross validation.

#### 3.4. Baseline Methods

**SVM:** The flattened upper triangle of the FC matrix is used as input to SVM.

**BrainNetCNN**(Kawahara et al., 2017b): An extension of CNNs to handle brain graph-structured data using special kernels.

**GroupINN** (Yan et al., 2019b): An ensemble of GCNs to learn graph-level latent embedding representations.

**ASD-DiagNet** (Eslami et al., 2019): Dense autoencoder for

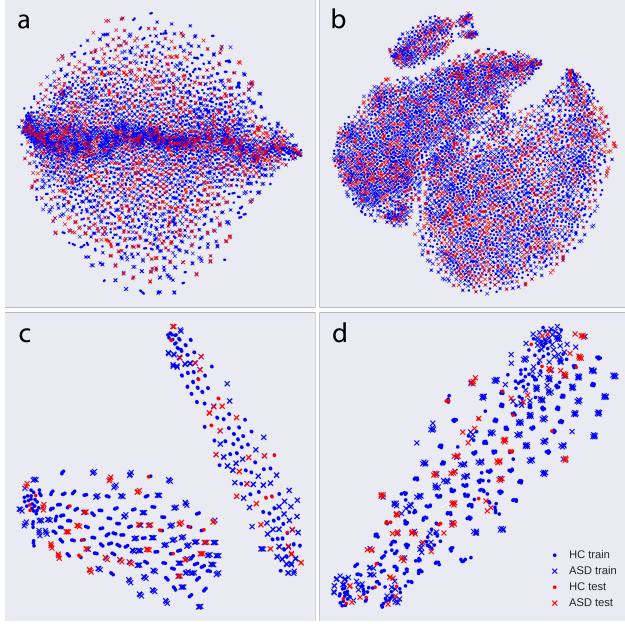


Figure 2. Top figures are t-SNE visualizations on the latent state sequences  $\{\mathbf{Z}_t\}_{t=0}^T$  of (a) graph recurrent autoencoder and (b) variational graph recurrent autoencoder, respectively. Bottom figures are t-SNE visualizations on the final (time-step) readouts  $\text{vec}([\mu_T^{\text{enc}}, \mu_T^{\text{H}}]^\top)$  of (c) variational graph recurrent autoencoder and (d) variational graph recurrent autoencoder with adversarial training, respectively.

embedding learning and single-layered perceptron for classification.

**Hi-GCN** (Jiang et al., 2020b): This method uses GroupINN to produce the embedding for all network instances, the learned embeddings are fed to a population-based GCN for classification.

**E-HI-GCN** (Li et al., 2021): An ensemble of HI-GCN, each of which is trained on different sparsity level brain networks.

**GAE-FCNN** (Noman et al., 2022): GAE is used to learn dynamic graph-level latent embeddings; the learned embeddings are fed to a FCNN for classification.

**GAE-LSTM** (Noman et al., 2022): The learned dynamic embeddings of GAE are fed to a LSTM for classification.

## 4. Results & Discussions

To evaluate the effectiveness of the proposed method, a nested-stratified 5-folds cross validation was applied for each experiment. The performance of ASD identification is measured using five metrics: accuracy, recall, precision, F1-score, and area under the curve (AUC). Table 1 compares the average performances of the proposed DSVB-FCNN with the existing baseline classifiers based on both dynamic and static FC networks. It shows that the proposed DSVB-FCNN achieves significant improvement over the baseline classifiers in each of the metrics. The proposed

DSVB-FCNN achieved low standard deviations in all metrics, demonstrating a strong consistency in its performances across the 5-folds cross validation. In general, these results indicate that the proposed framework facilitates robust brain disorder identification by generating graph latent embeddings that generalized well to unseen dynamic FC networks beyond the limited training dataset.

To provide insights on these performance gains of the proposed DSVB-FCNN, we conduct an in-depth ablation study where certain components (i.e., variational Bayes, spatial-aware GRU and adversarial training) of the DSVB framework are removed to highlight their distinctive contributions to the improved dynamic FC classification result. Table 2 tabulates the average performances of the ablation study based on five DSVB model variants. It shows that model I underperformed in comparison to other spatial-aware GRU-empowered models. This indicates the importance of the proposed spatial-aware GRU in endowing recurrent model the ability to capture rich spatiotemporal patterns crucial for dynamic network classification.

Figures 2a and 2b show the t-distributed Stochastic Neighbor Embedding (t-SNE) visualizations of respective latent state sequences  $\{\mathbf{Z}_t\}_{t=0}^T$  from models II and III of the ablation study. It shows that the latent state t-SNEs of model II are more concentrated towards the centre in comparison to the t-SNEs of model III which is more uniform. This indicates that the VB elements (KLD and reparameterization) facilitate learning of a smooth latent embedding space to better accommodate subject-level spatiotemporal variability across the dynamic FC networks. Nevertheless, due to incorporation of the prior model via KLD loss (11), VB-based models generate latent embeddings that are highly accustomed to the causal structure of the dynamic FC data. This aggravates model overfitting and increases the chance of false classification, resulting in a inferior performance of model III in Table 2 when compared to model II.

Figures 2c and 2d show the t-SNE visualizations of respective readouts  $\text{vec}([\mu_T^{\text{enc}}, \mu_T^{\text{H}}]^\top)$  from models III and V. In particular, Figure 2c shows that the model III divided the readout t-SNEs into two predominant clusters based on the causal structure of each dynamic FC data. On the contrary, t-SNEs of model V in Figure 2d are more regularized which demonstrates effectiveness of the proposed adversarial training strategy in learning indiscriminate latent embedding space that generalized well to unseen dynamic FC networks. The coordination between all components of the proposed DSVB framework produces superior ASD identification performance as shown in Tables 1 and 2.

In addition, we constructed higher-order dFC by correlating the DSVB-learned embeddings  $\mathbf{z}_{it}$  between pairs of nodes, and examined the dynamic connectivity states in ASD by applying K-means clustering of these dynamic net-

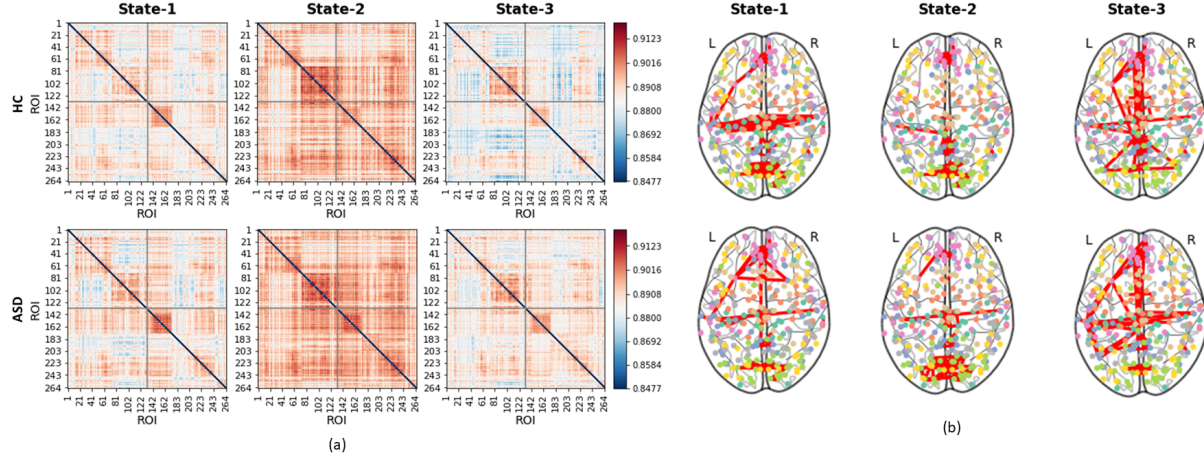


Figure 3. The average connectivity patterns as derived from the DSVB-learned embeddings. (a) 3 main states derived from K-means clustering of connectivity matrices from HC and ASD groups. (b) The corresponding connectome plots for HC and ASD.

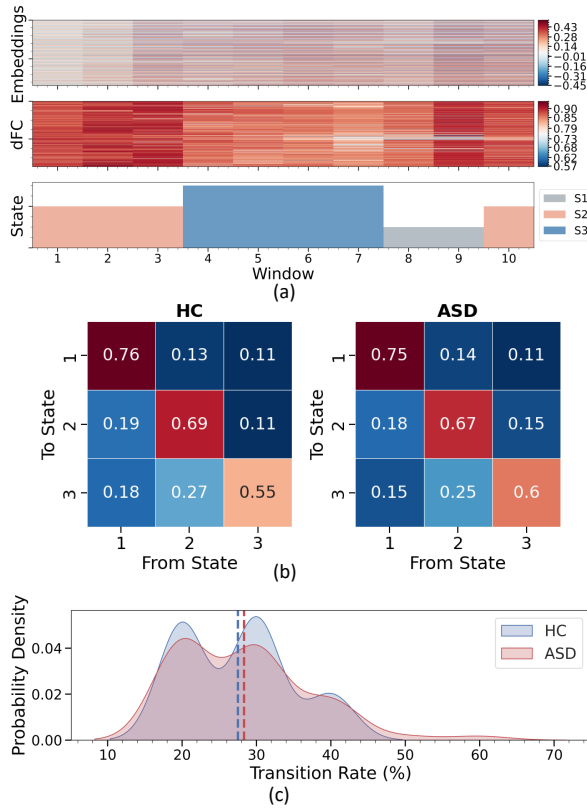


Figure 4. (a) The changes of states for a single HC subject. (b) The comparison of transition matrix between HC and AC for all subjects, this shows the average transition rate from one state to another. (c) The probability distribution of state transition rate for both HC and ASD.

works. Fig. 3 shows the estimated connectivity matrices for three different states with the corresponding highest FC connections. By referring to Power dictionary (Power et al., 2011), the corresponding brain functional system can be traced back. ASD group shows stronger FC connections in visual, default mode, salience networks; whereas higher

connectivity is observed in HC for sensory and auditory networks. The difference in FC patterns between ASD and HC are state-dependent. In ASD, visual ROIs shows increased interconnections in state-1 and state-2 where default mode and salience are mostly activated in state-1. This is consistent with previous findings (Holiga et al., 2019) that hyperconnectivity exists at prefrontal and parietal cortices; and hypoconnectivity restricted to sensory-motor regions for FC patterns in ASD as compared to HC.

Fig. 4 shows the analysis of the transitions between different brain states which has been modeled as a Markov chain. For subject  $i$ , the transition probability of moving from state  $k_1$  to state  $k_2$  is computed as  $P(s_{it} = k_2 | s_{i,t-1} = k_1)$  where  $s_{it}$  is the state of subject  $i$  at time point  $t$  estimated by k-means clustering. The continuance in the same states over time for both groups can be estimated using this transition probability. Notably, as compared to previous model (Noman et al., 2022), the DSVB-learned embeddings that account for spatiotemporal dependencies exhibit different patterns on the probability density of transition rates, it also shows that the ASD group exhibits more transitions compared to HC.

## 5. Conclusion

We developed a deep probabilistic spatiotemporal framework based on sequential variational Bayes for graph representation learning in dynamic FC networks for ASD identification. The proposed DSVB framework incorporates a spatial-aware GRU to capture both topological and temporal alterations across brain networks. A downstream FCNN then leverages the learned graph embeddings to reveal atypical neural connectivity patterns. Evaluation on resting-state fmri dataset with limited sample size shows significant improvements over the existing baseline methods, suggesting its potential in neuropsychiatric disorder identification.

## Software and Data

Code and data required to reproduce the results in this paper are provided in <https://anonymous.4open.science/r/Deep-Spatiotemporal-Variational-Bayes-92E6>.

## References

- Aedo-Jury, F., Schwalm, M., Hamzehpour, L., and Stroh, A. Brain states govern the spatio-temporal dynamics of resting-state functional connectivity. *Elife*, 9, 2020.
- Ahmadi, H., Fatemizadeh, E., and Motie-Nasrabadi, A. Identifying brain functional connectivity alterations during different stages of alzheimer’s disease. *Int. J. Neurosci.*, 132(10):1005–1013, 2022.
- Bronstein, M. M., Bruna, J., LeCun, Y., Szlam, A., and Vandergheynst, P. Geometric deep learning: Going beyond euclidean data. *IEEE Signal Process. Mag.*, 34(4):18–42, 2017.
- Cai, B., Zhang, G., Zhang, A., Xiao, L., Hu, W., Stephen, J. M., Wilson, T. W., Calhoun, V. D., and Wang, Y.-P. Functional connectome fingerprinting: Identifying individuals and predicting cognitive functions via autoencoder. *Hum. Brain Mapp.*, 42(9):2691–2705, 2021.
- Cameron, C., Sharad, S., Brian, C., Ranjeet, K., Satrajit, G., Chaogan, Y., Qingyang, L., Daniel, L., Joshua, V., Randal, B., Stanley, C., Maarten, M., Clare, K., Adriana, D. M., Francisco, C., and Michael, M. Towards automated analysis of connectomes: The configurable pipeline for the analysis of connectomes (C-PAC). *Front. Neuroinform.*, 7, 2013.
- Cao, W., Yan, Z., He, Z., and He, Z. A comprehensive survey on geometric deep learning. *IEEE Access*, 8:35929–35949, 2020.
- Chen, Z., Xia, M., Zhao, Y., Kuang, W., Jia, Z., and Gong, Q. Characteristics of intrinsic brain functional connectivity alterations in major depressive disorder patients with suicide behavior. *J. Magn. Reson. Imaging*, 54(6):1867–1875, 2021.
- Di Martino, A., Ross, K., Uddin, L. Q., Sklar, A. B., Castellanos, F. X., and Milham, M. P. Functional brain correlates of social and nonsocial processes in autism spectrum disorders: an activation likelihood estimation meta-analysis. *Biological psychiatry*, 65(1):63–74, 2009.
- Eslami, T., Mirjalili, V., Fong, A., Laird, A. R., and Saeed, F. ASD-DiagNet: a hybrid learning approach for detection of autism spectrum disorder using fMRI data. *Front. Neuroinform.*, 13:70, 2019.
- Filippi, M., Spinelli, E. G., Cividini, C., and Agosta, F. Resting state dynamic functional connectivity in neurodegenerative conditions: A review of magnetic resonance imaging findings. *Front. Neurosci.*, 13:657, 2019.
- Ganin, Y., Ustinova, E., Ajakan, H., Germain, P., Larochelle, H., Laviolette, F., Marchand, M., and Lempitsky, V. Domain-adversarial training of neural networks. *The journal of machine learning research*, 17(1):2096–2030, 2016.
- Hajiramezanali, E., Hasanzadeh, A., Narayanan, K., Duffield, N., Zhou, M., and Qian, X. Variational graph recurrent neural networks. In *Advances in Neural Information Processing Systems*, volume 32, 2019.
- Holiga, Š., Hipp, J. F., Chatham, C. H., Garces, P., Spooren, W., D’Ardhuy, X. L., Bertolino, A., Bouquet, C., Buitelaar, J. K., Bours, C., Rausch, A., Oldehinkel, M., Bouvard, M., Amestoy, A., Caralp, M., Gueguen, S., Ly-Le Moal, M., Houenou, J., Beckmann, C. F., Loth, E., Murphy, D., Charman, T., Tillmann, J., Laidi, C., Delorme, R., Beggato, A., Gaman, A., Scheid, I., Leboyer, M., d’Albis, M.-A., Seigney, J., Czech, C., Bolognani, F., Honey, G. D., and Dukart, J. Patients with autism spectrum disorders display reproducible functional connectivity alterations. *Sci. Transl. Med.*, 11(481), 2019.
- Hyde, K. K., Novack, M. N., LaHaye, N., Parlett-Pelleriti, C., Anden, R., Dixon, D. R., and Linstead, E. Applications of supervised machine learning in autism spectrum disorder research: a review. *Review Journal of Autism and Developmental Disorders*, 6(2):128–146, 2019.
- Jiang, H., Cao, P., Xu, M., Yang, J., and Zaiane, O. HiGCN: A hierarchical graph convolution network for graph embedding learning of brain network and brain disorders prediction. *Comput. Biol. Med.*, 127:104096, 2020a.
- Jiang, H., Cao, P., Xu, M., Yang, J., and Zaiane, O. HiGCN: A hierarchical graph convolution network for graph embedding learning of brain network and brain disorders prediction. *Comput. Biol. Med.*, 127:104096, 2020b.
- Kawahara, J., Brown, C. J., Miller, S. P., Booth, B. G., Chau, V., Grunau, R. E., Zwicker, J. G., and Hamarneh, G. BrainNetCNN: Convolutional neural networks for brain networks; towards predicting neurodevelopment. *Neuroimage*, 146:1038–1049, 2017a.
- Kawahara, J., Brown, C. J., Miller, S. P., Booth, B. G., Chau, V., Grunau, R. E., Zwicker, J. G., and Hamarneh, G. Brainnetcnn: Convolutional neural networks for brain networks; towards predicting neurodevelopment. *NeuroImage*, 146:1038–1049, 2017b.



- Khodatars, M., Shoeibi, A., Sadeghi, D., Ghaasemi, N., Jafari, M., Moridian, P., Khadem, A., Alizadehsani, R., Zare, A., Kong, Y., Khosravi, A., Nahavandi, S., Hus-sain, S., Acharya, U. R., and Berk, M. Deep learning for neuroimaging-based diagnosis and rehabilitation of autism spectrum disorder: A review. *Comput. Biol. Med.*, 139:104949, 2021.
- Kingma, D. P. and Welling, M. Auto-encoding variational bayes. In *International Conference on Learning Repre-sentations*, 2014.
- Lee, N. and Kim, J.-M. Dynamic functional connectivity analysis of functional MRI based on copula time-varying correlation. *J. Neurosci. Methods*, 323:32–47, 2019.
- Li, L., Jiang, H., Wen, G., Cao, P., Xu, M., Liu, X., Yang, J., and Zaiane, O. TE-HI-GCN: An ensemble of transfer hierarchical graph convolutional networks for disorder diagnosis. *Neuroinform.*, pp. 1–23, 2021.
- Li, L., Jiang, H., Wen, G., Cao, P., Xu, M., Liu, X., Yang, J., and Zaiane, O. TE-HI-GCN: An ensemble of transfer hierarchical graph convolutional networks for disorder diagnosis. *Neuroinformatics*, 20(2):353–375, 2022.
- Liu, J., Yao, L., Zhang, W., Deng, W., Xiao, Y., Li, F., Sweeney, J. A., Gong, Q., and Lui, S. Dissociation of fractional anisotropy and resting-state functional connectivity alterations in antipsychotic-naïve first-episode schizophrenia. *Schizophr. Res.*, 204:230–237, 2019.
- Liu, L., Wen, G., Cao, P., Hong, T., Yang, J., Zhang, X., and Zaiane, O. R. Braintgl: A dynamic graph representation learning model for brain network analysis. *Computers in Biology and Medicine*, 153:106521, 2023. ISSN 0010-4825. doi: <https://doi.org/10.1016/j.compbimed.2022.106521>.
- Moridian, P., Ghassemi, N., Jafari, M., Salloum-Asfar, S., Sadeghi, D., Khodatars, M., Shoeibi, A., Khosravi, A., Ling, S. H., Subasi, A., Alizadehsani, R., Gorriz, J. M., Abdulla, S. A., and Acharya, U. R. Automatic autism spectrum disorder detection using artificial intelligence methods with mri neuroimaging: A review. *Frontiers in Molecular Neuroscience*, 15, 2022. ISSN 1662-5099. doi: 10.3389/fnmol.2022.999605.
- Noman, F., Yap, S.-Y., Phan, R. C.-W., Ombao, H., and Ting, C.-M. Graph autoencoder-based embedded learning in dynamic brain networks for autism spectrum disorder identification. In *2022 IEEE International Conference on Image Processing (ICIP)*, pp. 2891–2895, 2022. doi: 10.1109/ICIP46576.2022.9898034.
- Nyatega, C. O., Qiang, L., Adamu, M. J., Younis, A., and Kawuwa, H. B. Altered dynamic functional connectivity of cuneus in schizophrenia patients: A Resting-State fMRI study. *NATO Adv. Sci. Inst. Ser. E Appl. Sci.*, 11 (23):11392, 2021.
- Power, J. D., Cohen, A. L., Nelson, S. M., Wig, G. S., Barnes, K. A., Church, J. A., Vogel, A. C., Laumann, T. O., Miezin, F. M., Schlaggar, B. L., and Petersen, S. E. Functional network organization of the human brain. *Neuron*, 72(4):665–678, 2011.
- RaviPrakash, H., Watane, A., Jambawalikar, S., and Bagci, U. Deep learning for functional brain connectivity: Are we there yet? In *Deep Learning and Convolutional Neural Networks for Medical Imaging and Clinical Informatics*, pp. 347–365. Springer International Publishing, 2019.
- Schumacher, J., Peraza, L. R., Firbank, M., Thomas, A. J., Kaiser, M., Gallagher, P., O’Brien, J. T., Blamire, A. M., and Taylor, J.-P. Dynamic functional connectivity changes in dementia with lewy bodies and alzheimer’s disease. *Neuroimage Clin*, 22:101812, 2019.
- Tanveer, M., Richhariya, B., Khan, R. U., Rashid, A. H., Khanna, P., Prasad, M., and Lin, C. T. Machine learning techniques for the diagnosis of alzheimer’s disease. *ACM Trans. Multimed. Comput. Commun. Appl.*, 16(1s):1–35, 2020.
- Valenti, M., Pino, M. C., Mazza, M., Panzarino, G., Di Paolantonio, C., and Verrotti, A. Abnormal structural and functional connectivity of the corpus callosum in autism spectrum disorders: a review. *Rev. J. Autism. Dev. Disord.*, 7(1):46–62, 2020.
- Vaswani, A., Shazeer, N., Parmar, N., Uszkoreit, J., Jones, L., Gomez, A. N., Kaiser, L. u., and Polosukhin, I. Attention is all you need. In *Advances in Neural Information Processing Systems*, volume 30, 2017.
- Wang, J., Wang, Y., Wu, X., Huang, H., Jia, Y., Zhong, S., Wu, X., Zhao, L., He, Y., Huang, L., and Huang, R. Shared and specific functional connectivity alterations in unmedicated bipolar and major depressive disorders based on the triple-network model. *Brain Imaging Behav.*, 14(1):186–199, 2020.
- Wang, Q., Li, H.-Y., Li, Y.-D., Lv, Y.-T., Ma, H.-B., Xiang, A.-F., Jia, X.-Z., and Liu, D.-Q. Resting-state abnormalities in functional connectivity of the default mode network in autism spectrum disorder: a meta-analysis. *Brain imaging and behavior*, pp. 1–10, 2021.
- Yan, Y., Zhu, J., Duda, M., Solarz, E., Sripada, C., and Koutra, D. GroupINN: Grouping-based interpretable neural network for classification of limited, noisy brain data. In *Proceedings of the 25th ACM SIGKDD International Conference on Knowledge Discovery & Data Mining*, pp. 772–782. Association for Computing Machinery, 2019a.

- Yan, Y., Zhu, J., Duda, M., Solarz, E., Sripada, C., and Koutra, D. GroupINN: Grouping-based interpretable neural network for classification of limited, noisy brain data. In *Proc. of the 25th ACM SIGKDD Int. Conf. on Knowledge Discovery & Data Mining*, pp. 772–782, 2019b.
- Yin, W., Li, L., and Wu, F.-X. A semi-supervised autoencoder for autism disease diagnosis. *Neurocomputing*, 483: 140–147, 2022.
- Zhang, L., Wang, M., Liu, M., and Zhang, D. A survey on deep learning for Neuroimaging-Based brain disorder analysis. *Front. Neurosci.*, 14:779, 2020.
- Zhou, H. and Zhang, D. Graph-In-Graph convolutional networks for brain disease diagnosis. In *2021 IEEE International Conference on Image Processing (ICIP)*, pp. 111–115, 2021.
- Zhu, D.-M., Yang, Y., Zhang, Y., Wang, C., Wang, Y., Zhang, C., Zhao, W., and Zhu, J. Cerebellar-cerebral dynamic functional connectivity alterations in major depressive disorder. *J. Affect. Disord.*, 275:319–328, 2020.